Electronic Supplementary Information

Reconstructing Bimetallic Carbide Mo_6Ni_6C for Carbon Interconnected MoNi Alloys to Boost Oxygen Evolution Electrocatalysis

Meng Yang Zu,[a] Chongwu Wang,[a] Le Zhang,[a] Li Rong Zheng[b] and Hua Gui Yang*[a]

[a.] Key Laboratory for Ultrafine Materials of Ministry of Education, School of Materials Science and Engineering, East China University of Science and Technology, Shanghai, 200237 (China)

[b.] Beijing Synchrotron Radiation Facility, Institute of High Energy Physics, Chinese Academy of Sciences, Beijing, 100049 (China)

* Corresponding author: hgyang@ecust.edu.cn (H. G. Y).

Experimental Section

Chemicals. Nickel nitrate hexahydrate ($Ni(NO_3)_2 \cdot 6H_2O$), ammonium molybdate tetrahydrate ($(NH_4)_6Mo_7O_{24} \cdot 4H_2O$), potassium hydroxide (KOH), sodium hydroxide (NaOH) and hydrochloric acid (HCl) were purchased from Shanghai Chemical Reagent Co. Ltd. Pt/C (5 wt% Pt on Vulcan carbon black) and was purchased from Alfa Aesar. Nafion (5 wt%) and glucose were obtained from Sigma-Aldrich. Iridium (IV) oxide (IrO_2) were obtained from Strem Chemicals, Inc. All chemicals were of analytical grade and used without any further purification. Ni foam was cleaned ultrasonically with acetone, ethanol, HCl solution (3.0 mol L^{-1}) and deionized (DI) water for 15 min respectively, to remove the oxide layers on the surface before use.

Synthesis of Mo_6Ni_6C/NF. The Mo_6Ni_6C/NF sample was fabricated by a hydrothermal method. First, 0.1000 g glucose, 0.5191 g $(NH_4)_6Mo_7O_{24} \cdot 4H_2O$ and 0.4362 g $Ni(NO_3)_2$ $6H_2O$ were dissolved in 30 mL DI water, following by sonicated at room temperature for approximately 30 min until a homogeneous solution was achieved. Then, the pre-treated Ni foam (1.6-mm thick, 110 p.p.i., geometric area of 1 cm^2) was placed against the wall of a 50 mL Teflon-lined stainless steel autoclave at a certain angle. The autoclave was sealed and heated at 150 ^oC for 6 h. After the hydrothermal reaction, the samples were completely washed with DI water and dried in a vacuum oven of 60 ^oC. Finally, the samples were annealed to obtain Mo_6Ni_6C/NF at 700 ^oC for 2 h under the mixture gas of H_2/Ar (v/v, 15/85) in a tube furnace.

Synthesis of O-MoNi-C/NF. To obtain O-MoNi-C/NF, a pre-oxidation step was first applied to the pristine Mo_6Ni_6C/NF electrode, using an electrochemical station in a three-electrode setup with Mo_6Ni_6C/NF as the anodic electrode. A potential of 1.6 V (all potentials were referenced to reversible hydrogen electrode) was applied to Mo_6Ni_6C/NF for 30 min. The initial electrode began to release bubbles after about 10 min. To characterize the components and structure of the material after pre-oxidation, a series of analyses were employed for the samples after 10 hours' chronopotentiometric test, including SEM, TEM, HAADF-STEM, XRD, XPS and XAFS.

Synthesis of NiMo alloy. $MoNi_4$ was prepared by a modified method[1]. Firstly, 0.5191 g $(NH_4)_6Mo_7O_{24} \cdot 4H_2O$ and 0.4362 g $Ni(NO_3)_2 \cdot 6H_2O$ were dissolved in DI water, and 1.0 M NaOH was dripped into the solution so as to control the pH of the solution to be ~ 9. Then, the obtained solid mixture was washed with water and ethanol, respectively, then drying at 60 ^oC in the vacuum oven. The sample was finally annealed at 400 ^oC under H_2/Ar (v/v, 20/80) for 2 h in a tube furnace.

Electrochemical measurements. The Mo_6Ni_6C/NF was directly used as the working electrode for electrochemical tests. For Pt/C, IrO_2, 30 mg of catalyst and 80 μL Nafion solution (5 wt%) were dispersed in 2 mL of 4:1 v/v water/ethanol by at least 30 min sonication to form a homogeneous ink. For $MoNi_4$/C sample, 30 mg catalyst combined with 10 mg carbon black and 80 μL Nafion solution (5 wt%) were dispersed in 2 mL of 4:1 v/v water/ethanol by at least 30 min sonication to form a homogeneous ink. The pretreated Ni foam was immersed into the ink for 30 s, and repeated for several times to obtain a mass loading of about 18 mg cm^{-2}, noted as Pt/C/NF, IrO_2/NF and $MoNi_4$/C/NF, as the working electrodes to test linear sweep voltammetry (LSV). All electrochemical studies were performed using an electrochemical station (CHI 660E) in a three-electrode setup with modified Ni foam electrodes as the working electrode, Ag/AgCl/KCl (3.5 M) electrodes as a reference electrode, graphite rod as a counter electrode, and electrolytes were de-aerated with argon before use. The electrocatalytic activities of the catalysts towards HER were examined by polarization curves with a scan rate of 5 mV s^{-1} in 1.0 M KOH at room temperature, And the electrocatalytic activities of the catalysts towards OER were examined by polarization curves with a scan rate of 1 mV s^{-1} in 1.0 M KOH at room temperature. All potentials were referenced to reversible hydrogen electrode (RHE) by following calculations: $E_{RHE} = E_{Ag/AgCl} + 0.059 \times pH + 0.205$. AC impedance measurements were carried out in the same configuration when the working electrode was biased at a certain overpotential from 10^5 Hz to 0.1 Hz with an AC voltage of 5 mV. All LSV curves and chronopotentiometric curves were corrected with *iR*-compensation (90%), and the equivalent series resistance (R_s) can be obtained from the EIS Nyquist plots as the first intercept of the main arc with the real axis. The stability test was conducted at the constant *j* of 10 mA cm^{-2}.

Calculation of ECSA. The ECSA was determined by measuring the capacitive current associated with double-layer charging from the scan-rate dependence of CVs. For this, the potential window of CVs was 0.3-0.34 V versus Ag/AgCl. The scan rates were 1 to 5 mV s^{-1}. The double-layer capacitance (C_{dl}) was estimated by plotting the $\Delta j = j_a - j_c$ at 0.32 V versus Ag/AgCl against the scan rate. The linear slope is twice of the double-layer capacitance C_{dl}, which is proportional to the ECSAs of the materials.

The value of ECSA (cm^2) was calculated as:

$$ECSA = C_{dl} / C_s$$

where Cs is the specific capacitance of the sample or the capacitance of an atomically smooth planar surface of the material per unit area under identical electrolyte conditions, and we temporarily use the C_s value of 0.04 mF cm^{-2} based on the previous literature[2, 3].

Evaluation of FE of O_2. The amount of evolved O_2 was measured by gas chromatography (RAMIN, GC2060) equipped with a thermal conductivity detector. Specifically, the Ar used as carrier gas of O_2 was continuously delivered into the anodic electrolyte at a rate of 5.00 mL min^{-1} and was routed into a gas chromatograph. Before measurement, a pre-oxidation process for electrochemical oxidation at 1.6 V for 30 min is applied to original Mo_6Ni_6C, using an electrochemical station in a three-electrode setup with Mo_6Ni_6C/NF as the anodic electrode to obtain O-MoNi-C. Then the chronopotentiometric test is applied to O-MoNi-C at j of 100 mA cm^{-2} for continuous OER process in 1.0 M KOH to measure Faradaic efficiencies. The volume fractions of O_2 in exhaust gas from anodic compartment at each potential were measured by gas chromatography every 5 min of electrolysis. The Faradaic efficiency of O_2 was calculated as below:

$$FE_{O_2} = \frac{4Fx_{O_2}pG}{IRT}$$

Where x_{O2} is the volume fraction of O_2 in the exhaust gas, I (A) is the steady-state total current, $G = 5$ mL min^{-1} is the Ar flow rate, $p = 1.013 \times 10^5$ Pa, $T = 273.15$ K, $F = 96485$ C mol^{-1}, $R = 8.3145$ J mol^{-1} K^{-1}.

Characterizations. The crystal structure was determined using X-ray diffraction (Bruker D8 Advanced Diffractometer with Cu Kα radiation). The morphologies of the catalysts were examined by scanning electron microscope (Hitachi S4800) and transmission electron microscope (JEM 2100, 200 kV). Furthermore, the chemical states of the elements in catalysts were studied by X-ray photoelectron spectroscopy (Kratos Axis Ultra DLD), and the binding energy of the C 1s peak at 284.8 eV was taken as an internal reference. Mo K-edge and Ni K-edge X-ray absorption fine structure were performed on the 1W1B beamline of the Beijing Synchrotron Radiation Facility, China, operated at ~ 200 mA and ~ 2.5 GeV. Mo foil, Ni foil, MoO_3 and NiO powder were used as reference samples.

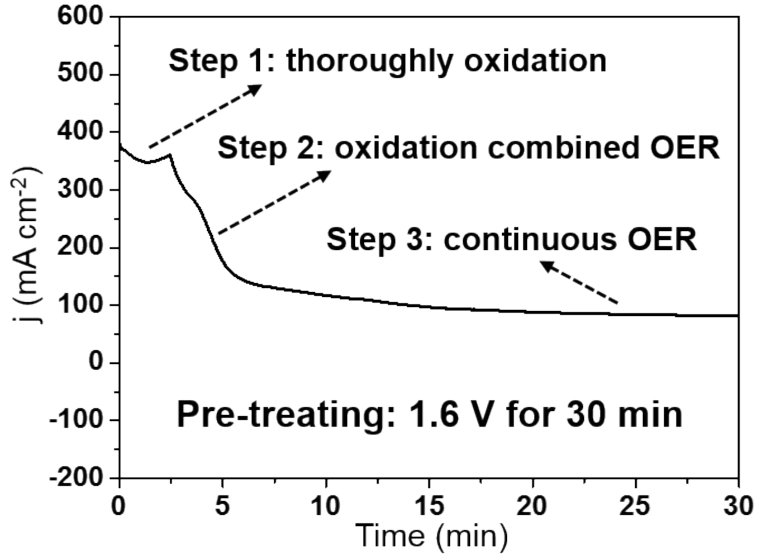

Fig. S1 I-t curve for the electrochemical oxidation at 1.6 V for 30 min. The curve mainly consists of three parts: During the first step, the current density is very high and almost keeps steady, revealing that the oxidation and the reconstruction processes are occurring in the the large unit cell of Mo_6Ni_6C; In the second step, the current density decreases as time goes on, implying that the reconstruction and the OER processes are taking place at the same time; For the third and last step, the current density reaches to a stable state without change, demonstrating that a continuous OER process occurred to generate O_2.

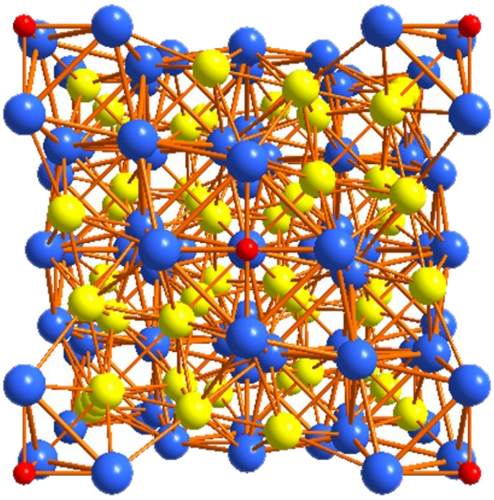

Fig. S2 Schematic representation of the structure of Mo_6Ni_6C (ICSD: 618328).

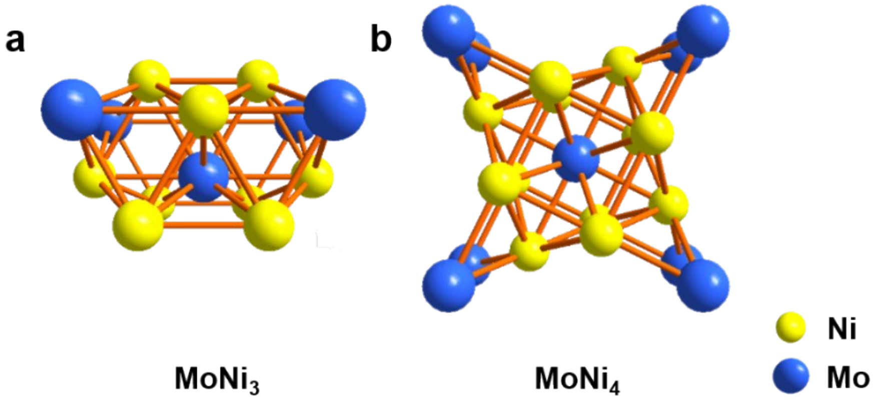

Fig. S3 Stick models of the $MoNi_3$ (ICSD: 1522820) and $MoNi_4$ (ICSD: 1523776).

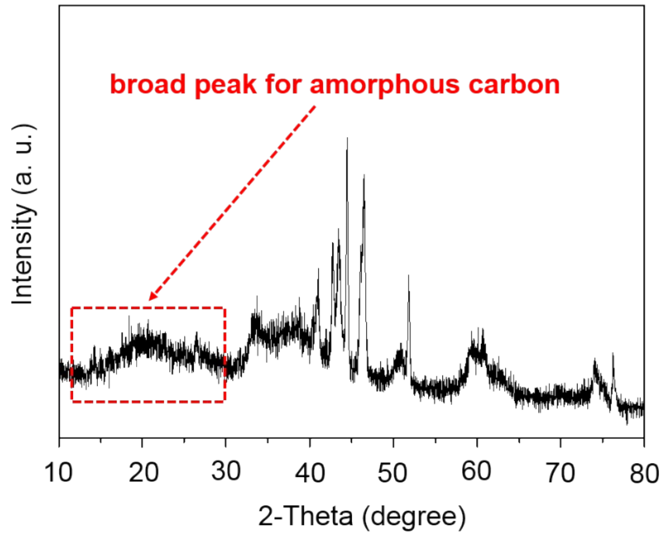

Fig. S4 XRD pattern of O-MoNi-C, revealing the amorphous structure for carbon[4].

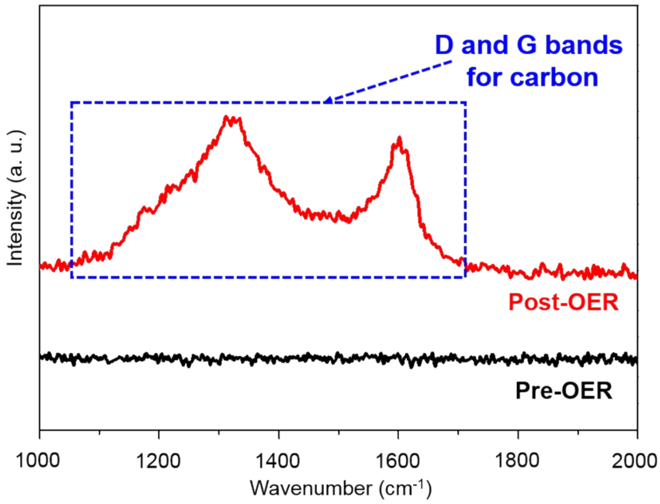

Fig. S5 Raman spectra for comparison of Mo_6Ni_6C (pre-OER) and O-MoNi-C (post-OER). The D band and G band correspond to the disordered graphitic carbon and graphitic carbon, respectively. The lower intensity of G band with respect to D band indicates the amorphous nature of the carbon component[5].

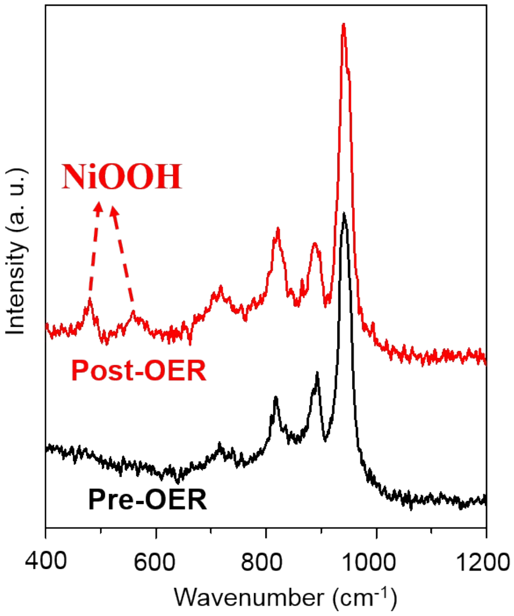

Fig. S6 Raman spectra of Mo_6Ni_6C (pre-OER) and O-MoNi-C (post-OER), revealing the formation of NiOOH on the surface during the OER process[6].

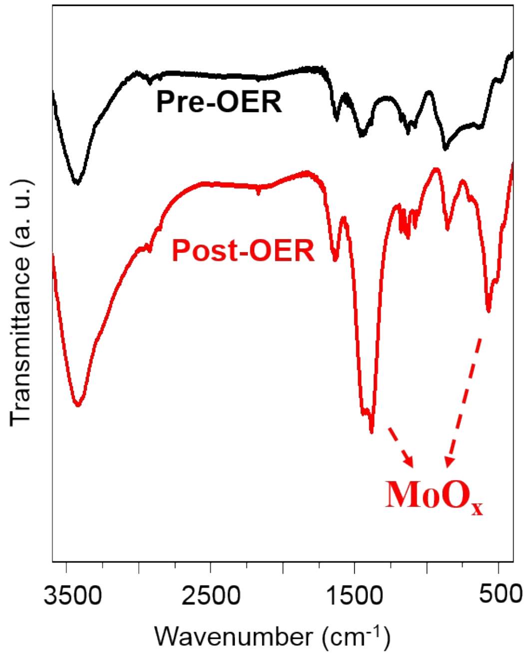

Fig. S7 FT-IR spectra of Mo_6Ni_6C (pre-OER) and O-MoNi-C (post-OER), demonstrating the formation of MoO_x on the surface during the OER process[7].

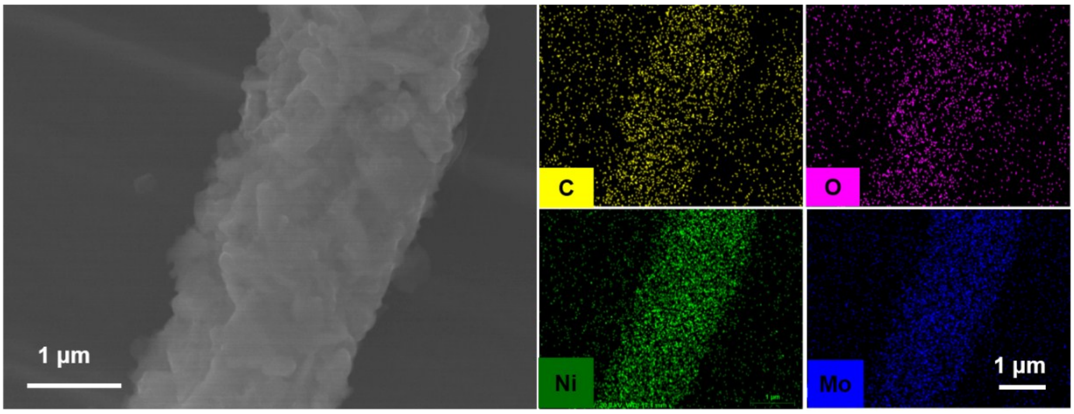

Fig. S8 SEM and corresponding elemental mapping images for the sample of O-MoNi-C.

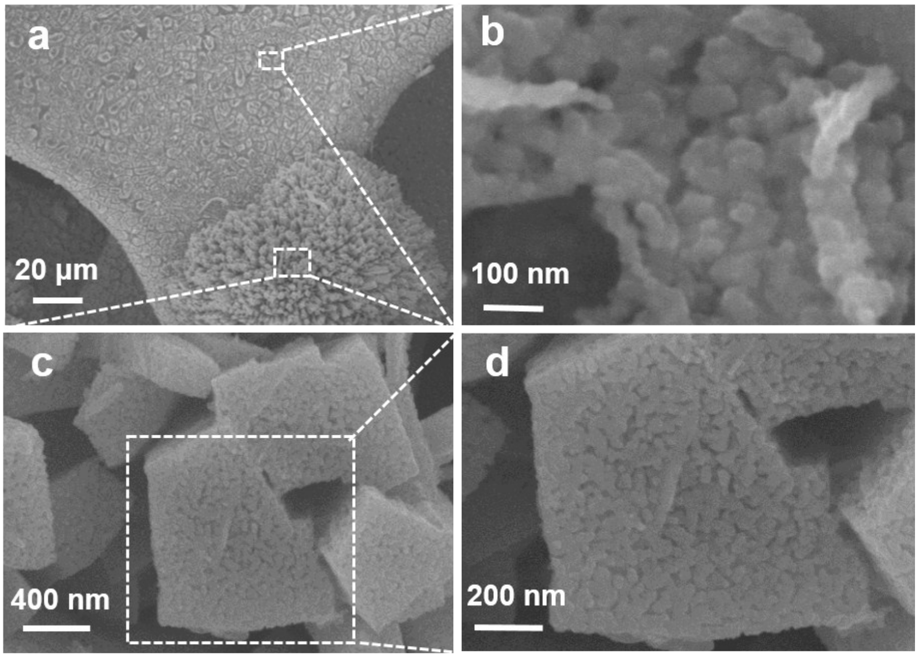

Fig. S9 SEM images of Mo_6Ni_6C-C/NF at different magnifications.

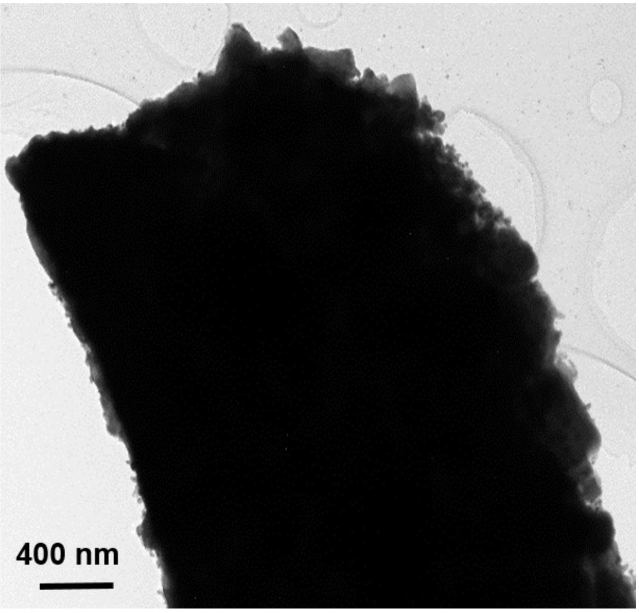

Fig. S10 TEM image of O-MoNi-C.

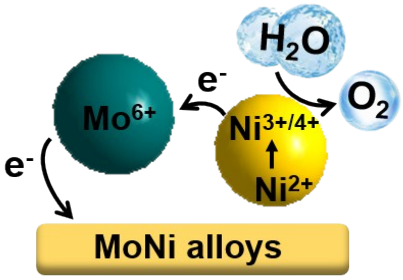

Fig. S11 Schematic representation of the effect for high-valence Mo^{6+} to activate 3d metal Ni active sites for OER.

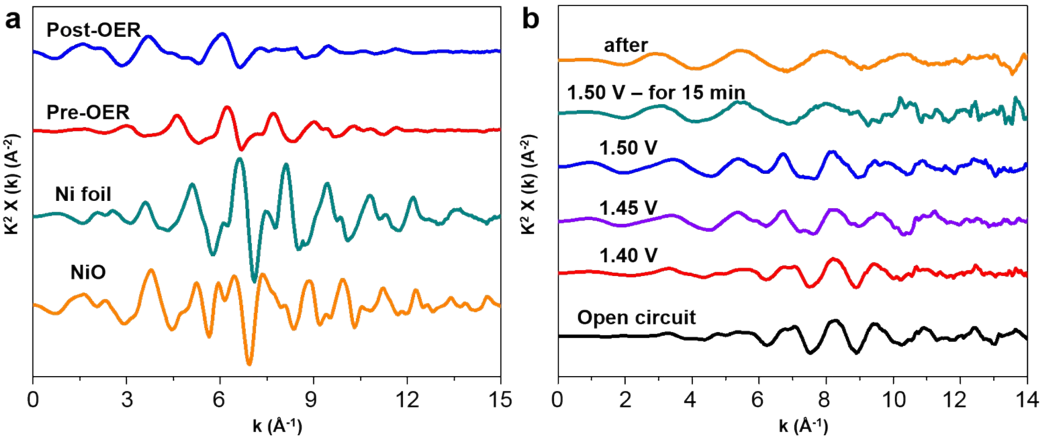

Fig. S12 The k^3-weighted spectra of (a) Mo_6Ni_6C (pre-OER), O-MoNi-C (post-OER), Ni foil, NiO for element Ni and (b) the samples under the work condition of in-situ OER process for element Mo.

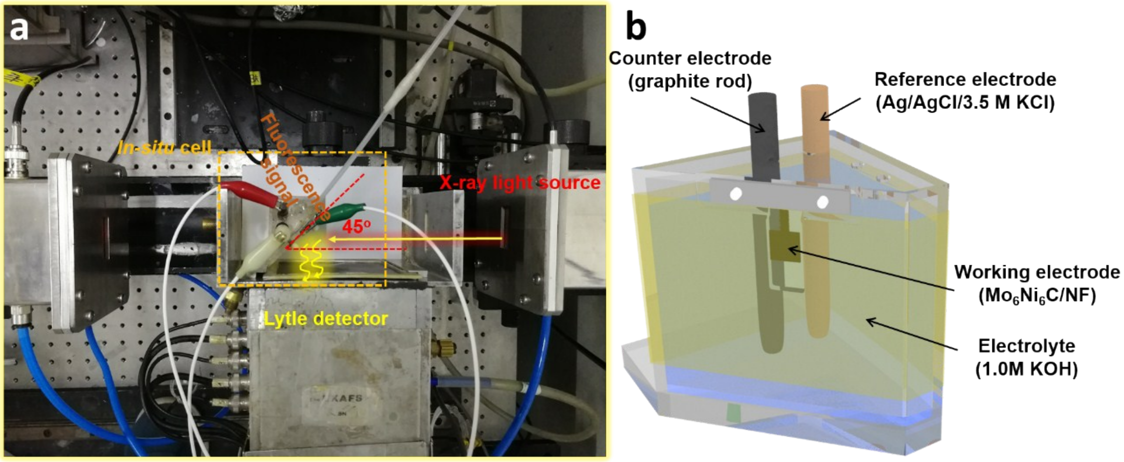

Fig. S13 (a) The typical experimental setup for in-situ XAFS measurements in transmission and fluorescence modes. (b) The schematic of the in-situ cell. The cell is wrapped with Teflon tape (yellow color) to guarantee the light transmission, and at the same time, to prevent the leakage of the electrolyte.

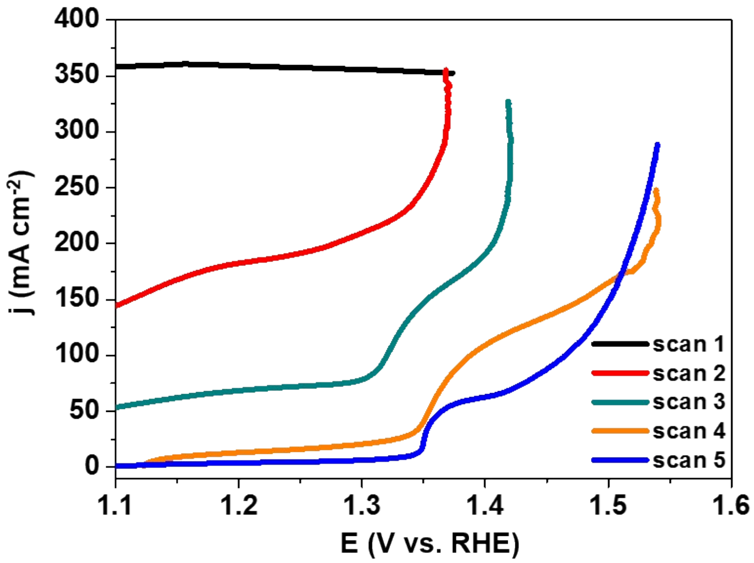

Fig. S14 LSV curves for Mo_6Ni_6C/NF repeating for several times. For the first scan, the current density is very high and almost keeps steady with potential increasing, implying that the oxidation and the reconstruction processes are occurring in the the large unit cell of Mo_6Ni_6C, and almost no OER process happens. For the second to fourth scans, the starting current density decreases as repeating scanning the LSV curves, revealing that the reconstruction process is gradually completing, and the OER process is taking place at the same time. For the fifth and last scan, the LSV curve reaches to a stable state, the keeps almost the same as O-MoNi-C/NF, which is obtained after the electrochemical oxidation at 1.6 V for 30 min.

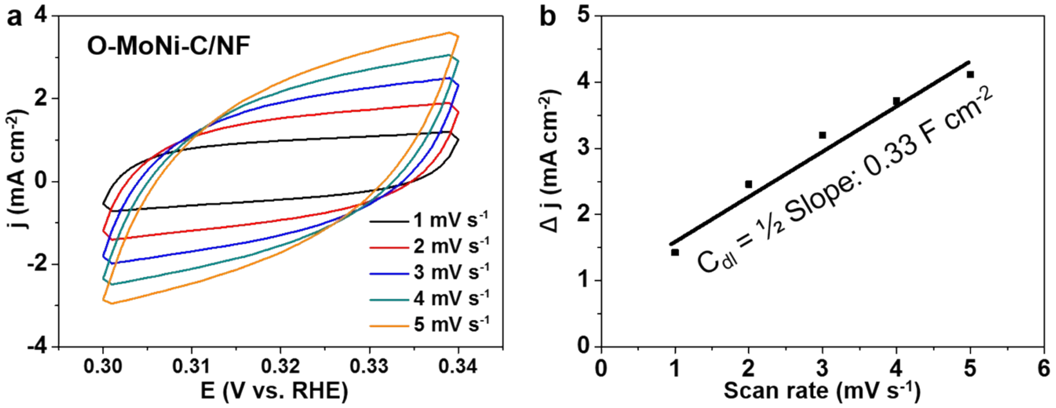

Fig. S15 The C_{dl} of O-MoNi-C/NF in 1.0 M KOH was assessed utilizing a series of cyclic voltammetry (CV) cycles at different scan rates. (a) Cyclic voltammograms of O-MoNi-C/NF at different scan rates (from 1 to 5 mV/s with an increment of 1 mV/s). (b) Scan rate dependence of the current densities ($\Delta j = j_a - j_c$) for O-MoNi-C/NF at 0.32 V vs Ag/AgCl.

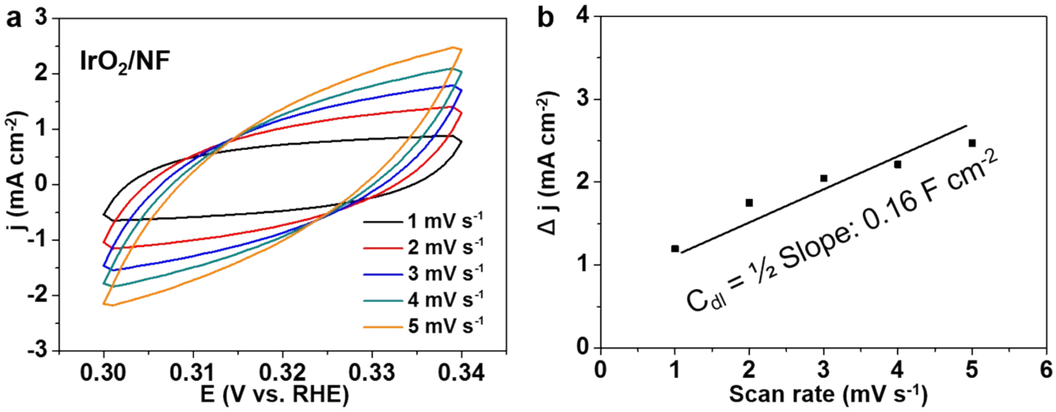

Fig. S16 The C_{dl} of IrO_2/NF in 1.0 M KOH was assessed utilizing a series of cyclic voltammetry (CV) cycles at different scan rates. (a) Cyclic voltammograms of O-MoNi-C/NF at different scan rates (from 1 to 5 mV/s with an increment of 1 mV/s). (b) Scan rate dependence of the current densities ($\Delta j = j_a - j_c$) for O-MoNi-C/NF at 0.32 V vs Ag/AgCl.

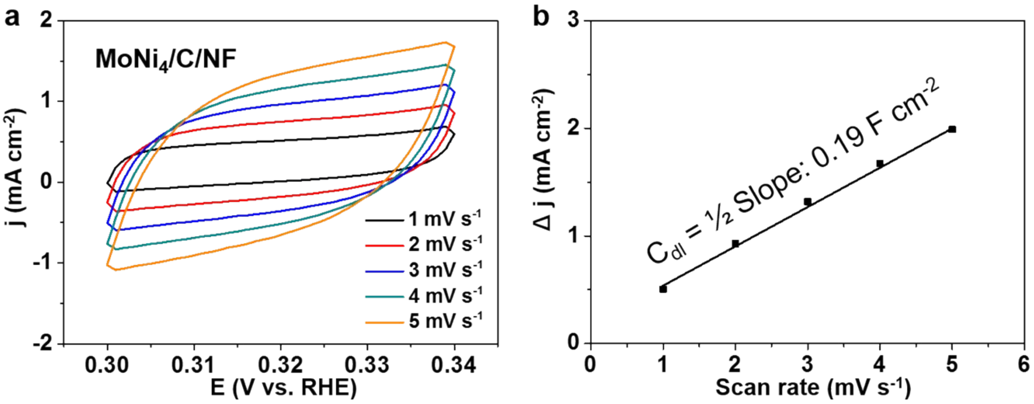

Fig. S17 The C_{dl} of $MoNi_4$/C/NF in 1.0 M KOH was assessed utilizing a series of cyclic voltammetry (CV) cycles at different scan rates. (a) Cyclic voltammograms of O-MoNi-C/NF at different scan rates (from 1 to 5 mV/s with an increment of 1 mV/s). (b) Scan rate dependence of the current densities ($\Delta j = j_a - j_c$) for O-MoNi-C/NF at 0.32 V vs Ag/AgCl.

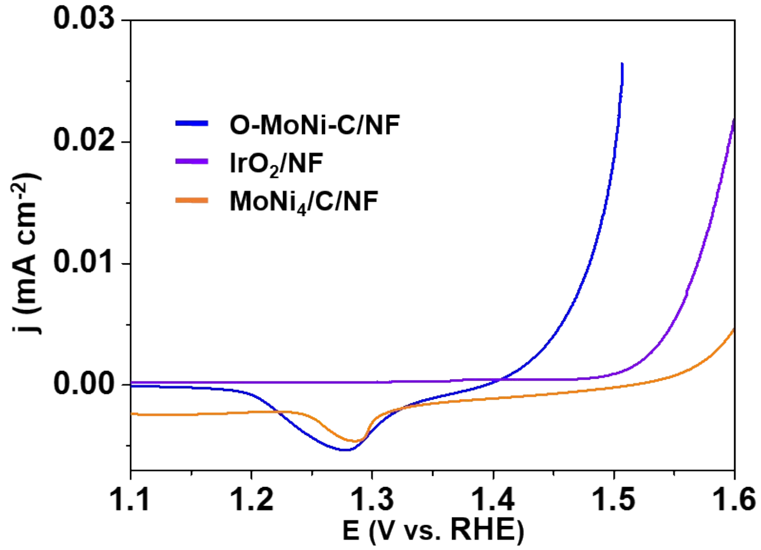

Fig. S18 The LSV curves normalized by ECSA for O-MoNi-C/NF and controlled samples (IrO$_2$/NF and MoNi$_4$/C/NF). Even normalized by ECSA, the *j* of O-MoNi-C/NF was still larger than that of compared samples (IrO$_2$/NF and MoNi$_4$/C/NF), further revealing that O-MoNi-C was intrinsically more active than compared samples.

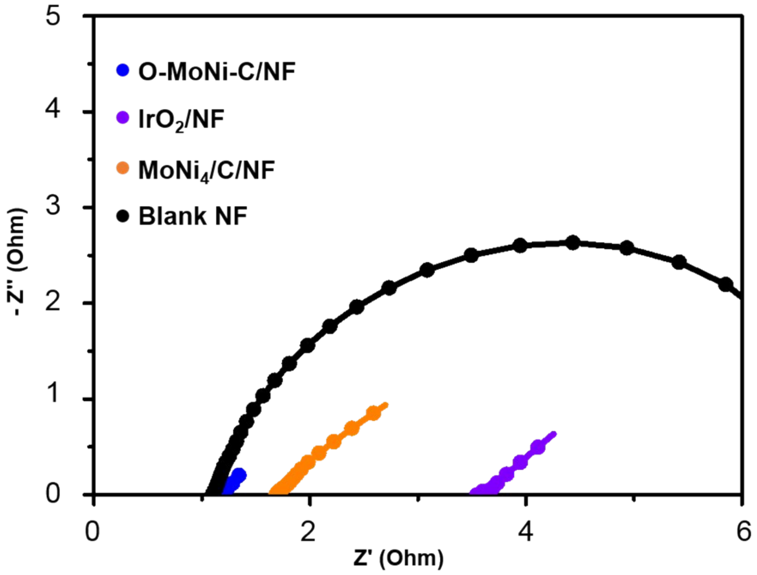

Fig. S19 Nyquist plots of O-MoNi-C/NF and other controlled samples.

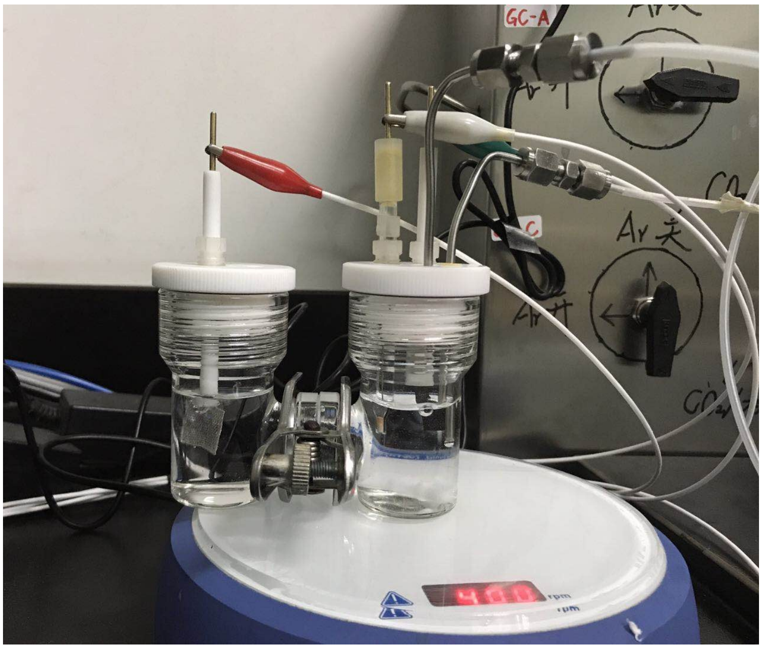

Fig. S20 A digital image showing the test conditions and experimental apparatus.

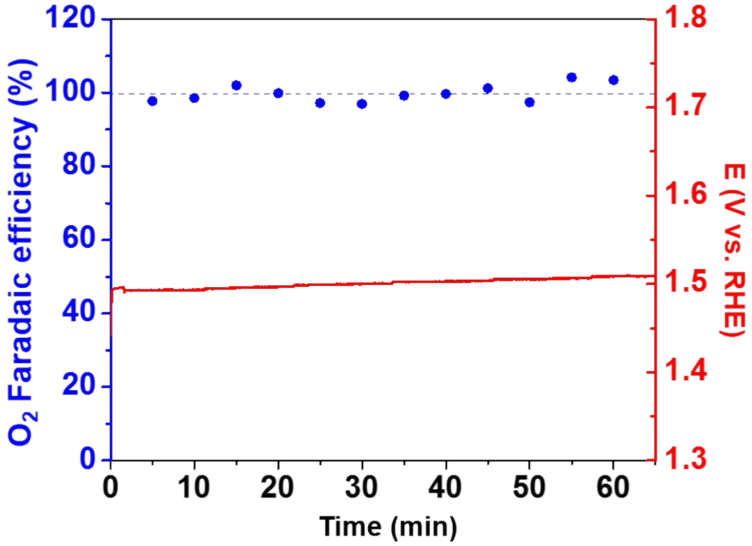

Fig. S21 Chronopotentiometric curve of O-MoNi-C/NF at *j* of 100 mA cm^{-2} for continuous OER process and the corresponding Faradaic efficiency from gas chromatography measurement of evolved O_2.

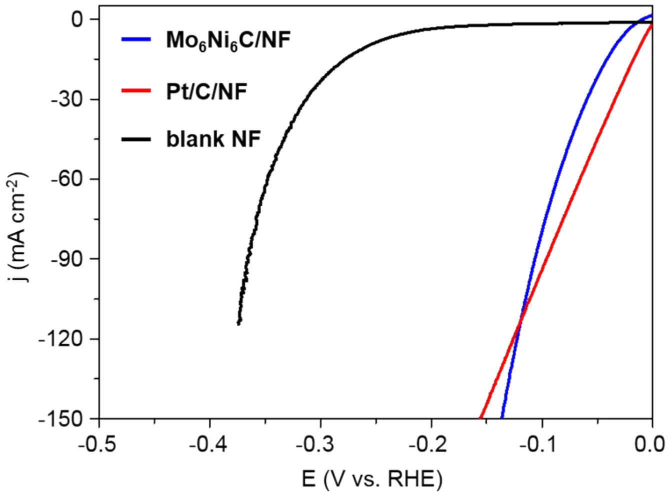

Fig. S22 LSV curves for HER in 1.0 M KOH for the samples of Mo$_6$Ni$_6$C/NF, Pt/C/NF and blank Ni foam.

Table S1. Comparison of electrocatalytic performance of O-MoNi-C and other OER electrocatalysts in 1.0 M alkali (KOH or NaOH) reported recently.

Materials	**Substrate**	**Mass loading ($mg\ cm^{-2}$)**	**η_{10} (mV)**	**Stability**	**Reference**
O-MoNi-C	Ni foam	9.80	190	100 h	this work
Ni_3N	GCE	~ 0.07	256	18 h	*Adv. Energy Mater.*, **2016**, *6*, 1601189.
Co-Fe-P NPs	GCE	~ 0.57	280	/	*Angew. Chem. Int. Ed.*, **2016**, *54*, 9642-9645.
Ni_3C	GCE	~ 0.29	316	15 h	*Adv. Mater.*, **2016**, *28*, 3326-3332.
$(Ni, Co)_{0.85}Se$	carbon fabric collector	~ 5.00	255	25 h	*Adv. Mater.*, **2016**, *28*, 77-85.
G-FeCoW	gold coated Ni foam	~ 0.21	191	500 h	*Science*, **2016**, *352*, 333-337.
$Ni_xFe_{1-x}Se_2$	Ni foam	~ 4.10	195	24 h	*Nat. Commun.*, **2016**, *7*, 12324.
NiCo-MOF	GCE	~ 0.20	250	/	*Nat. Energy*, **2016**, *1*, 16184.
$CoFe_2O_4/C$	Ni foam	~ 1.03	240	30 h	*Adv. Mater.*, **2016**, *29*, 1604437.
Co_4N	carbon cloth	/	310	20 h	*J. Am. Chem. Soc.*, **2016**, *138*, 10226-10231.
MAF-X27-OH	Cu foil	1.03	292	/	*J. Am. Chem. Soc.*, **2016**, *138*, 8336-8339.
$Ni(OH)_2$-Au	GCE	~ 0.27	270	/	*J. Am. Chem. Soc.*, **2016**, *138*, 9128-9136.
monolayer NiV-LDH	GCE	~ 0.14	318	25 h	*Nat. Commun.*, **2016**, *7*, 11981.
CoN	Ni foam	~ 1.50	290	30 h	*Angew. Chem. Int. Ed.*, **2016**, *55*, 8670-8674.
NiO/TiO_2	GCE	~ 0.34	320	10 h	*J. Am. Chem. Soc.*, **2016**, *138*, 6517-6524.
Gold-supported cerium-doped NiO_x	GCE	/	271	24 h	*Nat. Energy*, **2016**, *1*, 16053.
CoMnP	GCE	~ 0.28	330	/	*J. Am. Chem. Soc.*, **2016**, *138*, 4006-4009.
cobalt borate nanosheets/graphene	GCE	~ 0.29	290	/	*Angew. Chem. Int. Ed.*, **2016**, *55*, 2488-2492.

$CoSn(OH)_6$	carbon cloth	0.66	274	10 h	*Energy Environ. Sci.*, **2016**, *9*, 473-477.
Fe-Ni-O_x	GCE	0.10	286	/	*Angew. Chem. Int. Ed.*, **2014**, *53*, 7547-7551.
$Co_3O_4/NiCo_2O_4$	Ni foam	1.00	340	/	*J. Am. Chem. Soc.*, **2015**, *137*, 5590-5595.
Co_9S_8@MoS_2/CNFs	GCE	~ 0.21	430	/	*Adv. Mater.*, **2015**, *26*, 4752-4759.
Ni_5P_4 films	Ni foil	13.90	290	20 h	*Angew. Chem. Int. Ed.*, **2015**, *54*, 12361-12365.
NCNT/CoO-NiO-NiCo	GCE	0.21	270	/	*Angew. Chem. Int. Ed.*, **2015**, *54*, 9654-9658.
$NiFeO_x$/carbon nanofibres	CFP	~ 1.60	230	100 h	*Nat. Commun.*, **2015**, *6*, 7261.
ɣ-CoOOH nanosheets	GCE	~ 0.15	300	12 h	*Angew. Chem. Int. Ed.*, **2015**, *54*, 8722-8727.
$NiCo_2O_4$ ultrathin nanosheets	GCE	~ 0.29	320	/	*Angew. Chem. Int. Ed.*, **2015**, *54*, 7399-7404.
Co-P films	Copper foil	~ 1.00	345	24 h	*Angew. Chem. Int. Ed.*, **2015**, *54*, 6251-6254.
Ni_3N nanosheet	GCE	~ 0.29	256	18 h	*J. Am. Chem. Soc.*, **2015**, *137*, 4119-4125.
$NiCo_2O_4$	Ti foil	~ 0.30	370	20 h	*Adv. Energy Mater.*, **2015**, *5*, 1402031.
$NiCo_{2.7}(OH)_x$	GCE	~ 0.20	350	10 h	*Adv. Energy Mater.*, **2015**, *5*, 1401880.
FeNi LDH RGO	Ni foam	0.25	206	80 min	*Angew. Chem. Int. Ed.*, **2014**, *53*, 7584-7588.
NiFe-LDH (<5 nm)	GCE	0.28	210	30 h	*Adv. Mater.*, **2018**, *30*, 1705106.
$Ni_2P_4O_{12}$	carbon cloth	~ 3.30	270	100 h	*Adv. Mater.*, **2018**, *30*, 1705045.
FeCo-Co_4N/N-C	GCE	0.30	280	12 h	*Adv. Mater.*, **2017**, *29*, 1704091.
FeNiP	Ni foam	~ 4.12	180	25 h	*Adv. Mater.*, **2017**, *29*, 1704075.
Ni-Fe-Se cages	GCE	~ 0.10	240	22 h	*Adv. Mater.*, **2017**, *29*, 1703870.
CoO-MoO_2 nanocages	GCE	~ 0.50	312	15 h	*Adv. Funct. Mater.*, **2017**, *27*, 1702324.
vacancies rich CoFe LDH	GCE	~ 0.20	266	/	*Angew. Chem. Int. Ed.*, **2017**, *56*, 5867-5871.
NiFe LDH/CNT	GCE	~ 0.20	240	60 min	*J. Am. Chem. Soc.*, **2013**,

					135, 8452-8455.
NiCo-NS	GCE	~ 1.00	334	12 h	*Nat. Commun.,* **2014**, *5*, 4477.
CoMn-LDH	GCE	~ 0.14	324	14 h	*J. Am. Chem. Soc.,* **2014**, *136*, 16481-16484.

Note: 1. η_{10} represents the overpotential at the current density of 10 mA cm^{-2};

2. GCE is abbreviation for glassy carbon electrode;

3. CFP is abbreviation for carbon fiber paper.

Table S2. Comparison of the ECSAs for O-MoNi-C/NF and controlled samples (IrO_2/NF and $MoNi_4$/C/NF).

Samples	C_{dl} (F cm^{-2})	ECSA (cm^2)
O-MoNi-C/NF	0.33	8250
IrO_2/NF	0.16	4000
$MoNi_4$/C/NF	0.19	4477

Table S3. Comparison of overall water splitting performance of the electrolyzer constructed by Mo_6Ni_6C as both the OER pre-catalyst and HER catalyst and other bifunctional electrocatalysts in 1.0 M alkali (KOH or NaOH) reported recently.

Materials	**Mass loading (mg cm^{-2})**	**Type**	**η_{10} (mV)**	**Stability**	**V_{10} (V)**	**Stability for overall**	**Reference**
Mo_6Ni_6C		OER	190	100 h	1.47	200 h	this work
		HER	34	300 h			
NiFe LDH	/	OER	240	/	1.70	/	*Science*, **2014**, *345*, 1593-1596.
		HER	210	/			
$NiFeO_x$/carbon nanofibres	~ 3.00	OER	230	100 h	1.51	200 h	*Nat. Commun.,* **2015**, *6*, 7261.
		HER	88	/			
High-index Ni_3S_2	~ 1.60	OER	260	200 h	1.76 (13 mA·cm^{-2})	150 h	*J. Am. Chem. Soc.*, **2015**, *137*, 14023-14026.
		HER	223	200 h			
CoP	~ 2.00	OER	310	18 h	1.64	36 h	*J. Am. Chem. Soc.*, **2018**, *140*, 2610-2618.
		HER	115	20 h			
Ni-Co-P	2.00	OER	270	20 h	1.62	20 h	*Energy Environ. Sci.*, **2018**, 7, 872-880.
		HER	107	20 h			
Ni_2P	5.00	OER	290	/	1.63	10 h	*Energy Environ. Sci.*, **2015**, *8*, 2347-2351.
		HER	220	10 h			
NiSe	2.80	OER	< 270	12 h	1.63	20 h	*Angew. Chem. Int. Ed.*, **2015,** *54*, 9351-9355.
		HER	96	12 h			
Ni_5P_4	13.90	OER	330	20 h	<1.70	/	*Angew. Chem. Int. Ed.*, **2015**, *54*, 12361-12365.
MoS_2/Ni_3S_2 heterostructures	~ 13.10	OER	218	/	1.56	10 h	*Angew. Chem. Int. Ed.*, **2018,** *128*, 6814–6819.
		HER	110	/			
$NiCo_2O_4$ hollow microcuboids	~ 1.00	OER	290	32 h	1.65	36 h	*Angew. Chem. Int. Ed.*, **2016**, *55*, 6290-6294.
		HER	110	32 h			
BP/Co_2P	~ 0.14	OER	~ 370	24 h	~ 1.90	/	*Angew. Chem. Int. Ed.*, **2018**, *57*, 2600-2604.
		HER	~ 260	/			
h-NiS_x	142.20	OER	180	10 h	1.47	10 h	*Adv. Energy. Mater.*, **2016**, *6*, 1502333.
		HER	60	10 h			
$FePO_4$	~ 0.29	OER	218	14 h	1.54	14 h	*Adv. Mater.,* **2017**, *29*, 1704574.
		HER	123	/			
MoO_2 nanosheets	~ 3.40	OER	260	12 h	1.53	24 h	*Adv. Mater.*, **2016**, *28*, 3785-3790.
		HER	27	12 h			
Ni@NC	0.80	OER	280	10 h	1.60	50 h	*Adv. Mater.,* **2017**, *29*, 1605957.
		HER	205	10 h			
Co-P film	~ 1.00	OER	325	24 h	~1.58	24 h	*Angew. Chem. Int. Ed.,* **2015**, *54*, 6251-6254.
		HER	94	24 h			

$NiCo_2S_4$	/	OER	260	50 h	1.63	50 h	*Adv. Funct. Mater*., **2016**, *26*, 4661-4672.
		HER	210	50 h			
Ni_3FeN	~ 0.20	OER	280	9 h	/	/	*Adv. Funct. Mater*., **2016**, *6*, 1502585.
		HER	158	9 h			
two-tiered NiSe	/~	OER	290	30 h	1.69	/	*Adv. Energy. Mater*., **2018**, *8*, 1702704.
		HER	177	30 h			
NC/CuCo/ $CuCoO_x$	~ 1.50	OER	190	100 h	1.53	100 h	*Adv. Funct. Mater*., **2018**, *28*, 1704447.
		HER	119	100 h			
NiCo-HS@G	~ 1.50	OER	259	15 h	1.51	20 h	*Adv. Funct. Mater*., **2018**, *28*, 1704594.
		HER	51	/			
Ni-Fe-O nanowire	~6.10	OER	244	60 h	1.64	10 h	*Adv. Energy. Mater*., **2018**, *8*, 1701347.
		HER	/	/			

Note: 1. η_{10} represents the overpotential at the current density of 10 mA cm^{-2};

2. V_{10} represents the cell voltage of overall water splitting at the current density of 10 mA cm^{-2}.

References

1 K. Zhang, Y. Zhao, S. Zhang, H. Yu, Y. Chen, P. Gao and C. Zhu, *J. Mater. Chem. A*, 2014, **2***,* 18715-18719.

2 C. C. McCrory, S. Jung, J. C. Peters and T. F. Jaramillo, *J. Am. Chem. Soc.*, 2013, **135***,* 16977-16987.

3 P. Gu, L. Bai, L. Gao, R. Brousseau and B. E. Conway, *Electrochim. Acta*, 1992, **37***,* 2145-2154.

4 T. Y. Ma, S. Dai, M. Jaroniec and S. Z. Qiao, *J. Am. Chem. Soc.*, 2014, **136***,* 13925-13931.

5 H. B. Wu, B. Y. Xia, L. Yu, X.-Y. Yu and X. W. D. Lou, *Nat. Commun.*, 2015, **6***,* 6512.

6 W. Zhu, X. Yue, W. Zhang, S. Yu, Y. Zhang, J. Wang and J. Wang, *Chem. Commun.*, 2016, **52***,* 1486-1489.

7 L.-L. Feng, G. Yu, Y. Wu, G.-D. Li, H. Li, Y. Sun, T. Asefa, W. Chen and X. Zou, *J. Am .Chem. Soc.*, 2015, **137***,* 14023-14026.